

Ab-initio Exciton-polaritons: Cavity control of Dark Excitons in two dimensional Materials

Simone Latini,^{1,*} Enrico Ronca,^{1,†} Umberto De Giovannini,^{1,2,‡} Hannes Hübener,^{1,§} and Angel Rubio^{1,3,¶}

¹*Max Planck Institute for the Structure and Dynamics of Matter and
Center for Free Electron Laser Science, 22761 Hamburg, Germany*

²*Dipartimento di Fisica e Chimica, Università degli Studi di Palermo, Via Archirafi 36, I-90123, Palermo, Italy*

³*Center for Computational Quantum Physics (CCQ),
The Flatiron Institute, 162 Fifth Avenue, New York NY 10010.*

(Dated: October 8, 2018)

We demonstrate a robust and efficient way of controlling the optical spectra of two-dimensional materials by embedding them in a quantum cavity. The strength of the cavity light-matter coupling leads to superposition of bright and dark excitons making viable the optical observation of dark excitons. Our theoretical calculations are based on a newly developed theoretical framework that involves the ab-initio solution of the coupled quantized electron-photon Schrödinger equation in a quantum-electrodynamics plus Bethe-Salpeter approach. It enables the simulations of exciton-polariton states and their dispersion in a strong cavity light-matter coupling regime. We then develop a general Mott-Wannier model for this excitonic-polariton cavity problem which can be readily applied to a wider range of applications of van-der-Waals heterostructure materials in cavities.

PACS numbers: 78.20.Bh,78.67.-n,78.70.-g,42.50.Ct,42.50.Pq

Excitons dominate the optical properties of two-dimensional semiconductors. Single layers of Transition Metal Dichalcogenides (TMDs) have been under intense investigation for their excitonic properties [1–3]. Their weak electronic screening [4, 5], a consequence of the reduced dimensionality, leads to the formation of strongly bound excitons which play a fundamental role in a large variety of optoelectronic, spintronic and valleytronic properties [6]. Furthermore, single layers of TMDs can be stacked in multilayer crystals allowing for device engineering with a high degree of freedom [7–9]. Due to their strong coupling to electromagnetic radiation, TMD excitons represent ideal candidates to study strong light-matter coupling in optical cavities [10–14]. In an optical resonator, excitons interact with the quanta of light, generated by the spatial confinement of the cavity, resulting in the formation of new hybrid states with partial matter and light character, the *exciton-polaritons* [15–17]. These states are inherently different from the bare excitonic states in the material and therefore the appearance of a variety of novel phenomena can be expected. Envisioned examples, among others, comprise new topological phases [18], light-induced superconductivity [19], and exciton-polariton condensates [20].

Here, we present a first-principles theoretical framework, referred to as QED-BSE, designed to describe the coupling of excitonic states in solid state materials embedded in a quantum optical cavity. The method requires the exact diagonalization of an exciton-photon equation obtained by extending the widely used many-body Bethe-Salpeter (BSE) formalism [21–24] to the case of materials embedded in quantum cavities. This method is a many-body perturbation theory based alternative to the recently proposed quantum-electrodynamical density func-

tional theory [15–17, 25–30] that aims at describing the cavity mediated electron-photon interaction through effective functionals of the electron and photon densities. The current method can be used as a starting point to determine such functionals as done in the past for describing excitonic properties within time-dependent density functional theory [24]. In this work we demonstrate that by embedding a two-dimensional crystal in a cavity as sketched in fig.1, the optical activity of excitonic states can be controlled through cavity size and light-matter coupling strength. In dipole-approximation there are bright excitons (BE), i.e. accessible as direct transition from the groundstate upon photon absorption, and dark excitons (DE) which are instead not accessible in linear optical spectroscopy [31]. The inaccessibility of DE to standard spectroscopy poses a challenge for their detection and recent experimental and theoretical works have proposed sophisticated techniques to access them in TMDs [32]. Here we access DE through the coupling of the TMD crystal with a quantum cavity which allows direct transitions from the groundstate. Finally, we present an alternative computationally inexpensive method where we simplify the QED-BSE approach by substituting the BSE description of excitons with a hydrogenic Mott-Wannier (MW) model [33–35]. We show that the MW model accurately reproduces the results of the QED-BSE opening the way to the modeling of more complex systems in optical cavities, such as van-der-Waals heterostructures.

The electronic structure of a strongly coupled light-matter system in a cavity requires a non-perturbative treatment of the electron-photon interaction. Considering for simplicity a single cavity mode of frequency Ω , the long-wavelength (dipolar) electron-photon Hamilto-

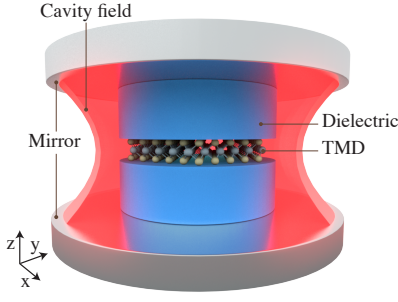


FIG. 1. Schematic representation of an encapsulated mono-layer TMD in an optical resonator (cavity).

nian for perfect loss-less cavity in velocity gauge reads:

$$\hat{H}_{\text{QED}} = \hat{H}_{\text{el}} + \Omega \hat{a}^\dagger \hat{a} + N_{\text{el}} \frac{A_0^2}{2} (\hat{a}^\dagger + \hat{a})^2 + A_0 \sum_{ijk} \left(\langle \phi_{i\mathbf{k}} | \hat{e} \cdot \hat{p} | \phi_{j\mathbf{k}} \rangle \hat{d}_{i\mathbf{k}}^\dagger \hat{d}_{j\mathbf{k}} \hat{a}^\dagger + h.c. \right), \quad (1)$$

where a^\dagger and a are the photon creation and annihilation operators respectively, \hat{H}_{el} the many-body electronic Hamiltonian, $\hat{d}_{i\mathbf{k}}^\dagger, \hat{d}_{j\mathbf{k}}$ the electronic creation and annihilation operators (with i, j band indices and \mathbf{k} wavevectors in the first Brillouin zone), \hat{p} the single particle momentum operator, N_{el} the number of electrons, \hat{e} the polarization of the photon and A_0 is the vector potential amplitude. Since the coupling of photons to the electronic structure occurs via the creation/annihilation of neutral electron-hole pairs, it is natural to approximate the eigenstates of the many-body electronic Hamiltonian by its excitonic eigenstates, i.e. $\hat{H}_{\text{el}} |\Psi_n^{\text{exc}}\rangle \simeq \epsilon_n^{\text{exc}} |\Psi_n^{\text{exc}}\rangle$. Under the approximation that the electron-hole Coulomb interaction that binds the exciton is not affected by the photons in the cavity, i.e. the screened Coulomb interaction is not dressed by the cavity photons, the QED Hamiltonian can be expanded in the excitonic basis as follows:

$$\langle \Psi_n^{\text{exc}} | \hat{H}_{\text{QED}} | \Psi_m^{\text{exc}} \rangle = \left[\epsilon_n^{\text{exc}} + \Omega \hat{a}^\dagger \hat{a} + N_{\text{el}} \frac{A_0^2}{2} (\hat{a}^\dagger + \hat{a})^2 \right] \delta_{nm} + A_0 (\mathcal{M}_{nm}^{\text{exc}} \hat{a}^\dagger + \mathcal{M}_{mn}^{\text{exc}*} \hat{a}), \quad (2)$$

where $\mathcal{M}_{nm}^{\text{exc}} = \sum_{ijk} \langle \phi_{i\mathbf{k}} | \hat{e} \cdot \hat{p} | \phi_{j\mathbf{k}} \rangle \langle \Psi_n^{\text{exc}} | \hat{d}_{i\mathbf{k}}^\dagger \hat{d}_{j\mathbf{k}} | \Psi_m^{\text{exc}} \rangle$ are excitonic matrix elements of the bilinear electron-photon coupling.

The excitonic states can be expressed as a linear combination of singly excited electronic determinants, where the coefficients of the linear combination are given by the solution of the BSE [22–24], $|\Psi_n^{\text{exc}}\rangle = \sum_{cv\mathbf{k}} A_{cv\mathbf{k}}^n \hat{d}_{c\mathbf{k}}^\dagger \hat{d}_{v\mathbf{k}} |\Psi_0\rangle$ with $A_{cv\mathbf{k}}^n$ the BSE coefficients, or envelope functions and c and v indices running over conduction and valence bands respectively. The elec-

tronic groundstate $|\Psi_0\rangle$ can instead be written as a single determinant of only valence states and we define $|\Psi_{n=0}^{\text{exc}}\rangle = |\Psi_0\rangle$.

In this work we consider the non-dispersive (momentum independent) excitonic states localized around the K-points of the Brillouin zone, which are the most relevant for the optoelectronic properties of TMDs. These excitonic states occur in two spin-orthogonal non-hydrogenic series, each of which is accurately described by a spin-independent two-band BSE, where only a single valence and a single conduction band are taken into account [35]. With this simplification the matrix elements appearing in Eq. (2) have one of the two following structures:

$$\mathcal{M}_{0n}^{\text{exc}} = \sum_{\mathbf{k}} A_{\mathbf{k}}^n \langle \phi_{v\mathbf{k}} | \hat{e} \cdot \hat{p} | \phi_{c\mathbf{k}} \rangle \quad (3)$$

$$\mathcal{M}_{nm}^{\text{exc}} = N_{\text{el}} \sum_{\mathbf{k}} A_{\mathbf{k}}^{m*} A_{\mathbf{k}}^n [\langle \phi_{c\mathbf{k}} | \hat{e} \cdot \hat{p} | \phi_{c\mathbf{k}} \rangle - \langle \phi_{v\mathbf{k}} | \hat{e} \cdot \hat{p} | \phi_{v\mathbf{k}} \rangle] \quad (4)$$

The matrix elements of the form Eq. (3) are those that dictate the dark/bright nature of the excitonic state. Those that have the form of Eq. (4), instead, are mixing the character of the excitonic states so that bright to dark or dark to bright transitions can occur.

Below we show first principles results for MoS_2 obtained by first solving the BSE with the GPAW code [36, 37] (see supplementary material for calculation details) and subsequently diagonalizing the QED Hamiltonian of Eq. (2) in a mixed exciton-photon product state basis $|\Psi_n^{\text{exc}}\rangle \otimes |\gamma\rangle$, where $|\gamma\rangle$ are the eigenfunctions of the photonic harmonic oscillator. We then extract energies ($E_I^{\text{pol}}(\Omega)$) and corresponding eigenfunctions ($|\Psi_I^{\text{pol}}(\Omega)\rangle = \sum_{ln} C_{ln}^I |\Psi_n^{\text{exc}}\rangle \otimes |\gamma\rangle$) for the exciton-polariton eigenstates. As for the photonic part, we consider the first non-zero photon mode ($\Omega = \pi c/L_\perp$) with out-of-plane wavevector and in-plane electric field in order to be able to couple to the MoS_2 excitons. For our quasi-2D cavity configuration the vector potential amplitude A_0 is frequency independent, unlike in the 3D case, indeed $A_0 = 1/\sqrt{SL_\perp\Omega} = 1/\sqrt{2\pi cS}$, where S is the in-plane area of the cavity. Furthermore we stress that the single mode approximation is valid for polaritons with energies lower than the energy of the second photon mode ($\Omega = 2\pi c/L_\perp$). In the supplementary material we show that including higher energy modes does not change the conclusions discussed below. We note that diagonalization of Eq. (2) is equivalent to solving a CI-singles in the presence of a photon mode. In particular, excited states of the material are expressed as linear combinations of singly excited determinants starting from the ground state and subsequently coupled, through the diagonalization, to the photonic degrees of freedom.

In order to visualize the experimentally measurable exciton-polariton dispersion, we calculate the matter

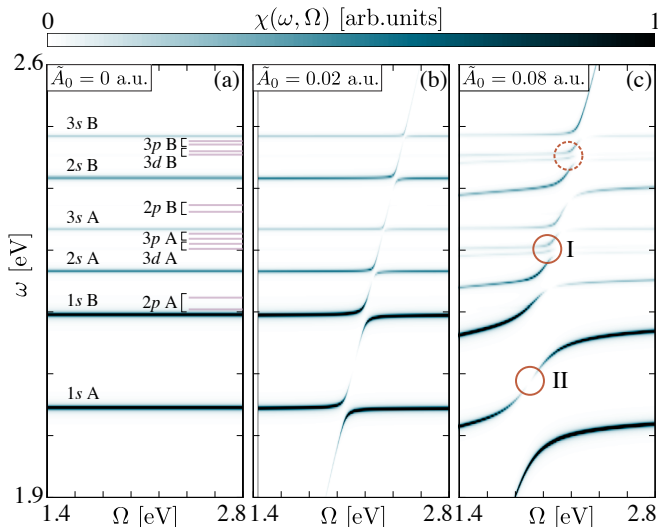


FIG. 2. Exciton-polariton spectra of MoS₂ in a cavity as a function of cavity mode frequency Ω and for three different coupling strength \tilde{A}_0 in a.u.. (a) For no coupling to the cavity mode the optical spectrum displays a series of spin-orbit split A and B excitons where only excitons with s symmetry appear, i.e. are bright. DE are reported in red segments. (b) For weak coupling excitons hybridize with the cavity photon to form exciton polaritons resulting in Rabi splitting of the bright exciton lines. (c) For strong coupling the Rabi splitting becomes more pronounced and additional polariton features appear where bright polariton branches cross dark exciton states. The broadening parameter used for the plots is $\eta = 5 \cdot 10^{-5}$ a.u..

component of the optical response $\chi(\omega, \Omega)$ applying linear response theory on the polaritonic states[30]:

$$\chi(\omega, \Omega) = \sum_I \frac{\mathcal{M}_{0I}^{\text{pol}} \mathcal{M}_{I0}^{\text{pol}}}{\omega - E_I^{\text{pol}}(\Omega) - E_0^{\text{pol}}(\Omega) + i\eta} \quad (5)$$

where $\mathcal{M}_{IJ}^{\text{pol}} = \langle \Psi_I^{\text{pol}} | \hat{p} | \Psi_J^{\text{pol}} \rangle = \sum_{lmn} C_{ln}^{I*} C_{mn}^J \mathcal{M}_{lm}^{\text{exc}}$. The formation of exciton-polaritons results in a richer optical response as compared to the bare excitonic response. In Fig. 2 we show the cavity polariton spectrum of MoS₂ as a function of mode energy and for different coupling strength $\tilde{A}_0 = A_0/N_{\text{el}}$. Here the coupling strength arises from a microscopic definition while in practice it can be controlled by the cavity geometry manufacturing parameters [38].

Without any electron-photon coupling ($\tilde{A}_0 = 0$), the spectrum features only the bare BEs, characterized by the common spin-orbit split A and B exciton series (see supplementary material)[39]. Bound excitons in TMDs have atom like spherical symmetries, following the usual pattern of s, p, d angular momentum quantum numbers and consequently are subject to atomic like selection rules [32]. Only excitons with s -type symmetry are accessible from the ground state through direct absorption of photons. The p and d -type excitons instead can be classified

as DEs.

In the weak coupling regime (c.f. Fig. 2(b)) the formation of an exciton-polariton is accompanied by the characteristic avoided crossing in the energy dispersion, which results from the hybridisation between the linear dispersing photon branch and the non-dispersive exciton branches. For a given cavity frequency within the hybridisation region, this is detectable as a splitting of the exciton peak into two separate peaks – the Rabi splitting.

For stronger coupling (c.f. Fig. 2(c)), the interaction between the cavity photon and the DE results in the appearance of new spectral features marked by circles in the figure. Specifically, we can identify additional splittings (I)/interruptions (II) signature of a cavity induced optical modulation. In this strong coupling regime ($\tilde{A}_0 = 0.08$) we performed calculations also for different TMDs (MoSe₂, WS₂ and WSe₂, see supplementary material) observing qualitatively equivalent features. It is worth noting that for the first exciton of WS₂ we obtain a Rabi splitting of ≈ 22 meV in line with experimental values measured by Flatten et al. ($\approx 20 - 70$ meV)[10]. While it is hard to assess the exact coupling conditions under which the experiment has been performed, this comparison shows that the coupling values used here are on the lower end of the experimentally accessible values.

Further insight into the structure of these dark polaritons is provided by the analysis shown in Fig. 3. The panels quantify the contribution of the different excitonic states to the optically active polariton states at specific cavity energy along the dispersion branches shown in Fig. 2. The decomposition of the polariton in Fig. 3(a), which is a zoom-in of the circle (I) in fig.2(c), shows that it is predominantly the $3d$ DE that is creating the polaritonic eigenstate. However, it is only because of the photon mediated coupling to the $2s$ BE that the $3d$ DE acquires a finite optical cross section. More specifically the coupling between the two states happens within the $\gamma = 0$ photon sector meaning that there is not an actual absorption or emission of photons in the mixing process but rather both an absorption and subsequent emission (or vice versa) to and from a virtual p -like state. As demonstrated by the insets in Fig. 3(a) both the lower and upper branch of the DE polariton have a similar composition.

While Fig. 3(a) illustrates how the cavity coupling reveals hidden (dark) states of a material, we observe another peculiarity in the polariton dispersion in Fig. 3(b), which corresponds to the circle (II) in fig.2(c). Through the cavity we can induce a quench of the optical activity within the polariton branch connecting two BEs, i.e. the spectral response vanishes completely between two consecutive BE lines. In this case, such a dimming of the polariton branch is *not* originating from the contribution of DE states, but instead is the result of destructive interference between the optical transition amplitudes from the exciton lines connected by the photon branch. The

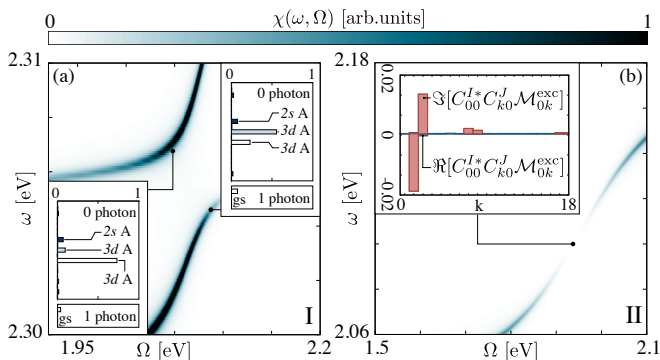


FIG. 3. (a) Enlarged view of the dark exciton for the region highlighted in Fig. 2 by I. The insets show the composition of the polariton eigenstates (see text) for points on the lower and upper branch. (b) Enlarged view of a point where the polariton vanished exactly between two consecutive bright exciton lines, highlighted in Fig. 2 by II. The inset shows the real and imaginary parts of the matrix elements contributing to this feature (see text).

destructive interference is demonstrated in the inset of Fig. 3(b) which reports the real and imaginary part of the transition amplitude from the groundstate to the 1s A and 1s B excitonic states, which are the states that make up most of the polariton state.

The QED-BSE method illustrated above requires considerable computational effort and it is therefore limited to few layers of lattice matched TMDs. The polaritonic physics can be well reproduced by replacing the BSE part in the QED-BSE with the Mott-Wannier (MW) equation, hence considerably reducing the computational cost and more importantly giving access to exciton-polariton physics in more complex materials such as encapsulated 2D crystals and van-der-Waals heterostructures. In particular it provides a computationally inexpensive way of assessing the effect of the dielectric in which the optically active material is embedded [35] (as sketched in the cartoon in Fig. 1). In this approach the bound excitons are described by a hydrogen like Schrödinger equation that provides the exciton envelope functions and hence allows the evaluation of the exciton-dipole matrix elements $\mathcal{M}_{mn}^{\text{exc}}$ of the QED-BSE approach. The effect of a dielectric substrate is accounted for in the MW description through its bulk dielectric constant κ , c.f. Refs. [35 and 40] and supplementary material for a detailed description of the method. The effect of environmental screening is threefold: (i) extra-screening of the electron-hole Coulomb interaction, (ii) renormalized photon dispersion ($\omega = \omega_c/\sqrt{\kappa}$) which now propagates in dielectric medium and (iii) by renormalizing the effective vector potential amplitude of the cavity $\bar{A}_0(\kappa) = \tilde{A}_0/\kappa$ [33].

In Fig. 4(a) we show the polariton dispersion of MoS₂ for fixed coupling strength \tilde{A}_0 and for various values of dielectric constants for the substrate material κ . The most striking feature is the change in the slope of the

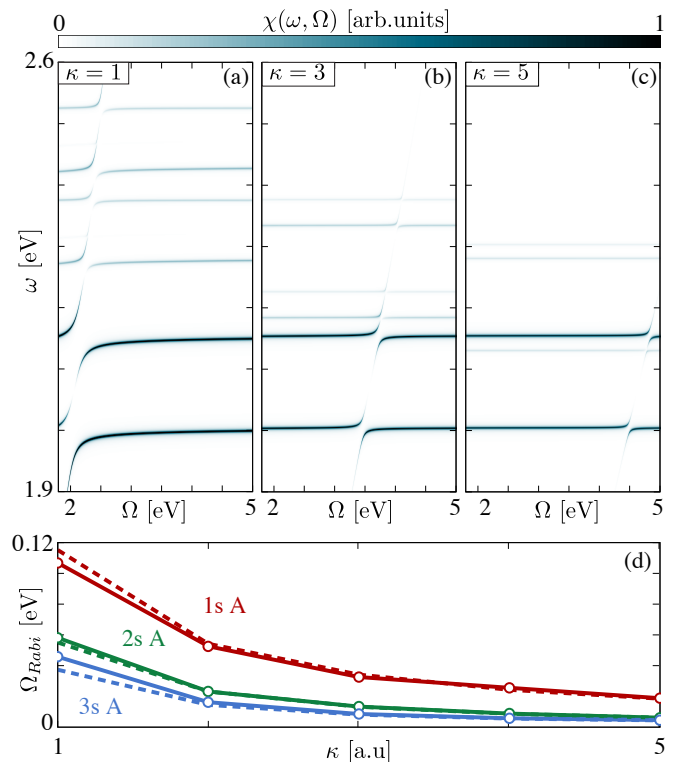


FIG. 4. Polariton dispersion of MoS₂ for different values of dielectric constant κ of the substrate (a-c), calculated with the MW model and with $\tilde{A}_0 = 0.05$. Dependence of the Rabi splitting of the 1s A, 2s A and 3s A states on the dielectric constant (d). Solid lines with circles are the Rabi splitting calculated with the MW model, dashed lines are calculated from the Jaynes-Cummings model as $\Omega_{\text{Rabi}} = 2A_0\mathcal{M}_{0n}^{\text{exc}}$.

photon line due to the propagation in the cavity dielectric. This shifts the position of the polariton resonances. Furthermore, due to the change of the screened Coulomb interaction, the higher lying excitons are squeezed in energy towards the first excitonic state (cf. supplementary material). Fig. 4(c) shows the dependence of the Rabi splitting of the first three BEs (1s, 2s, 3s of the A series) as a function of the dielectric constant of the encapsulating material. We compare the splitting of the calculated dispersion with the Rabi splitting of the corresponding Jaynes-Cummings model where only two levels at a time (the groundstate and one of the excitons) are taken into account. Notably, only for small dielectric constants there are deviations from Jaynes-Cummings splitting indicating that for larger effective couplings \tilde{A}_0 the two level approximation breaks down.

a dressing of more than a single excitonic state in the MW method.

The QED-BSE formalism we presented here is a first principles approach to the properties of polaritons in optical cavities. We show how it gives rise to complex polaritons dispersions, where hybridizations of polaritons manifest in features originating from DE. We show how

to use the Mott-Wannier model for bound excitons to obtain the relevant dipole matrix elements that enter the QED equations and thus provide a readily applicable model to compute such polariton properties. This model can be extended to account for the dielectric screening of materials inside the cavity which gives access to a large variety of van-der-Waals layered systems. The QED-BSE and MW model presented here are the first ab-initio methods aimed at the design and understanding of cavity control of optoelectronic materials properties.

ACKNOWLEDGEMENTS

S.L. and E.R. equally contributed to the work.

We are grateful for helpful discussions with Ch. Schäfer, M. Sentef and M. Ruggenthaler. S. L. acknowledges support from the Alexander von Humboldt foundation. We further acknowledge financial support from the European Research Council(ERC-2015-AdG-694097) and European Union H2020 program under GA no.676580 (NOMAD). The Flatiron Institute is a division of the Simons Foundation.

SUPPLEMENTARY MATERIAL

QED-BSE Computational Details

All of the ab-initio calculations for the electronic problem in this work are performed with the GPAW code [36, 37]. The single particle energies and wavefunctions, together with the momentum matrix elements $\langle \phi_{i\mathbf{k}} | \hat{e} \cdot \hat{p} | \phi_{j\mathbf{k}} \rangle$ are calculated within density functional theory with the LDA exchange correlation functional on a plane-wave basis. The LDA calculations for the monolayers TMDs were performed using a plane wave basis set with a cut off energy of 500 eV and 60×60 k-point grids.

We calculate the excitonic wavefunctions to be used in the QED Hamiltonian by solving the BSE considering only electron-hole pairs formed between the top valence and bottom conduction band. We take a cut-off energy of 150 eV for the evaluation of the screened interaction, which is calculated within the RPA on LDA energies and wavefunctions. A scissor operator based on the G_0W_0 calculations is applied for a better description of the electronic gap, see Tab. I for specific values. Spin-orbit effects are included post BSE solution by including two equivalent spin-orthogonal (A and B) excitonic series. Spin-orbit splitting values are reported in Tab. I. The Brillouin zone sampling for BSE and G_0W_0 calculations is done on a 60×60 k-point-mesh.

Finally, in the QED Hamiltonian 18 excitonic states (up to the 3s) and only one photon mode are included

TMD	GW gap (eV)	SOC split (eV)
MoS ₂	2.53	0.15
MoSe ₂	2.14	0.17
WS ₂	2.60	0.37
WSe ₂	2.21	0.40

TABLE I. GW band gap and SOC splittings for different TMDs. All values are extracted from the C2DB two-dimensional materials database [41]

and the exciton-polariton dispersion is converged with a photon number $\gamma = 3$ for the energy region and \tilde{A}_0 values investigated here. Exciton-polariton dispersions for MoS₂, WS₂, MoSe₂ and WSe₂ are shown in Fig. 5

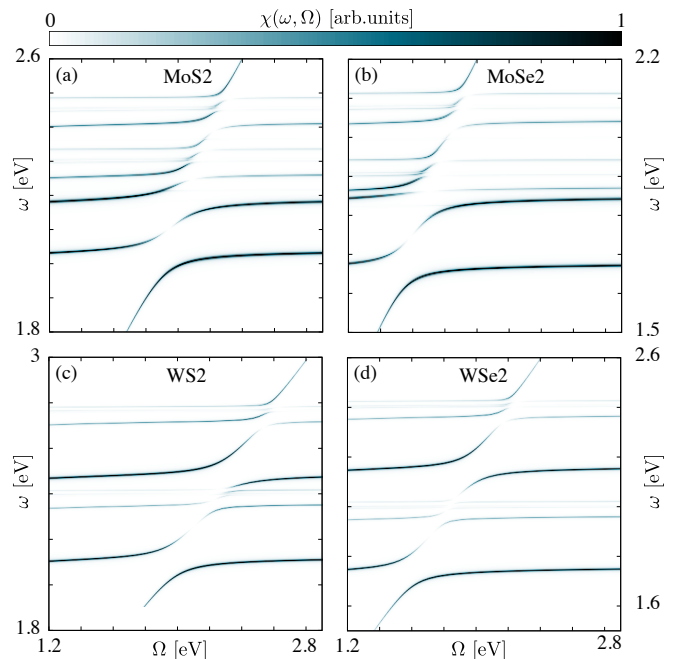


FIG. 5. Exciton polariton dispersion of different TMDs with a coupling constant of $\tilde{A}_0=0.08$ a.u..

QED-BSE Multi-mode Calculations

To avoid unnecessary complications, in the main text we only treated a single cavity mode. Eq. (1) of the main text can be directly generalized to the case of multiple

modes, in formulas:

$$\begin{aligned} \hat{H}_{\text{QED}} = & \hat{H}_{\text{el}} + \sum_{\mathbf{q}\sigma} \Omega_{\mathbf{q}} \hat{a}_{\mathbf{q}\sigma}^\dagger \hat{a}_{\mathbf{q}\sigma} + \\ & \frac{N_{\text{el}}}{2} \sum_{\mathbf{q}\sigma} A_{0\mathbf{q}\sigma}^2 |(u_{\mathbf{q}\sigma}^* \hat{a}_{\mathbf{q}\sigma}^\dagger + u_{\mathbf{q}\sigma} \hat{a}_{\mathbf{q}\sigma})|^2 + \\ & \sum_{\mathbf{q}\sigma} A_{0\mathbf{q}\sigma} \sum_{ijkk'} \left(\langle \phi_{i\mathbf{k}} | u_{\mathbf{q}\sigma}^* \hat{p}_\sigma | \phi_{j\mathbf{k}'} \rangle \hat{d}_{i\mathbf{k}}^\dagger \hat{d}_{j\mathbf{k}'} \hat{a}_{\mathbf{q}\sigma}^\dagger + h.c. \right), \end{aligned} \quad (6)$$

where \mathbf{q} is the photon momentum, σ the x, y, z index and $u_{\mathbf{q}\sigma}$ the photon polarization vectors. In a quasi-2D cavity the latter are given by:

$$\begin{aligned} u_{\mathbf{q}x} = u_{\mathbf{q}y} = & e^{i\mathbf{q}_{\parallel} \cdot \mathbf{r}_{\parallel}} i \sin(q_{\perp} z), \\ u_{\mathbf{q}z} = & e^{i\mathbf{q}_{\parallel} \cdot \mathbf{r}_{\parallel}} \cos(q_{\perp} z). \end{aligned} \quad (7)$$

In our work the relevant quantization dimension is the out-of-plane one and we only consider photon modes for which $\mathbf{q}_{\parallel} = 0$. We then assume that the active 2D crystal has an infinitesimal thickness and it is placed at the center of the cavity, namely $z = L_{\perp}/2$. Given the isotropy of TMDs monolayers, we can choose the in plane polarization to be in the y -direction, without any loss of generality. In such a setting and because 2D excitons can only couple to in-plane electric fields we consider only polarization of the kind $u_{\mathbf{q}y} = i \sin(q_{\perp} L_{\perp}/2)$ and of these only the odd modes are non-zero, i.e. $q_{\perp} = \frac{\pi\alpha}{L_{\perp}}$ with $\alpha = 1, 3, 5, \dots$. With the restriction of the modes just described, the longwavelength approximation can be still applied and we can simplify the Hamiltonian in Eq. 6 as:

$$\begin{aligned} \hat{H}_{\text{QED}} = & \hat{H}_{\text{el}} + \sum_{\alpha} \Omega_{\alpha} \hat{a}_{\alpha}^\dagger \hat{a}_{\alpha} + \frac{N_{\text{el}}}{2} \sum_{\alpha} A_{0\alpha}^2 |(\hat{a}_{\alpha}^\dagger + \hat{a}_{\alpha})|^2 + \\ & \sum_{\alpha} A_{0\alpha} \sum_{ijk} \left(\langle \phi_{i\mathbf{k}} | \hat{e} \cdot \hat{p} | \phi_{j\mathbf{k}} \rangle \hat{d}_{i\mathbf{k}}^\dagger \hat{d}_{j\mathbf{k}} \hat{a}_{\alpha}^\dagger + h.c. \right), \end{aligned} \quad (8)$$

with $\Omega_{\alpha} = \alpha\pi c/L_{\perp}$ and $A_{0\alpha} = 1/\sqrt{2\pi c S} \sqrt{\alpha}$.

Following the procedure we used for the single mode case, we project the Hamiltonian above onto the product state basis $|\Psi_n^{\text{exc}}\rangle \otimes |\gamma^{\alpha=1}\rangle \otimes |\gamma^{\alpha=3}\rangle \otimes \dots$, where $|\gamma^{\alpha}\rangle$ are the eigenfunctions of the photonic harmonic oscillator associated with the different modes. The Hamiltonian can be then diagonalized and the resulting polaritonic states and energy can be used for calculating the optical response as in Eq. (5) of the main text. Calculations for MoS₂ with up to $\alpha = 7$ are reported in Fig. 6. Within the Ω range considered in the main text the multi-mode calculation is in quantitative agreement with the single-mode one. However including more modes allows us to explore smaller values of Ω , where polaritonic effects due to the smaller modes take place.

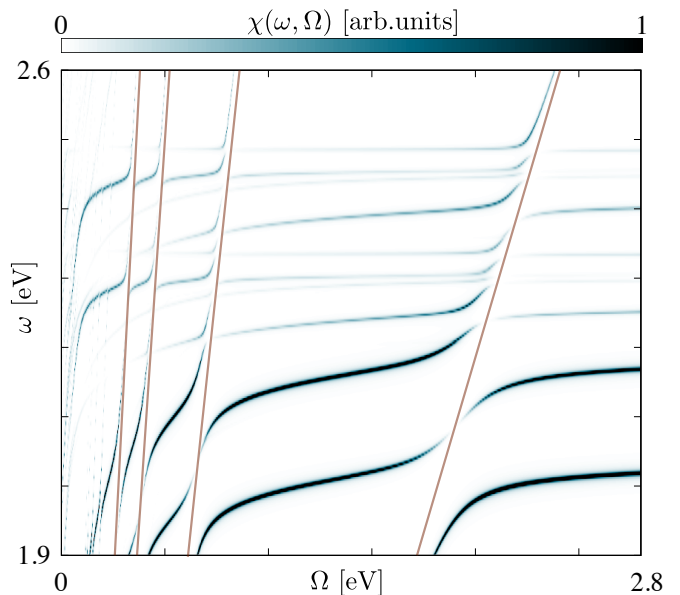


FIG. 6. Exciton-polariton spectra of MoS₂ in a cavity as a function of cavity mode frequency Ω obtained with a multi-mode model with up $\alpha = 7$ modes and a coupling strength of $\tilde{A}_0 = 0.08$ a.u..

MW Method and Computational Details

In the MW model, the exciton is treated as a hydrogen atom, where the electron and the hole interact via a screened Coulomb interaction, described by the Schrödinger equation [35]

$$\left[-\frac{\nabla^2}{2\mu} - W(\mathbf{r}) \right] F^n(\mathbf{r}) = E_{b,\text{exc}}^n F^n(\mathbf{r}). \quad (9)$$

with μ the exciton effective mass and the screened Coulomb interaction

$$W(\mathbf{r}) = \frac{1}{4\alpha} [H_0(x) - N_0(x)]_{x=r/2\pi\alpha}, \quad (10)$$

where H_0 and N_0 are the Struve and Neumann functions and α is the crystal polarizability. By solving Eq. (9), we obtain exciton binding energies ($E_{b,\text{exc}}^n = E_{\text{gap}} - E_{\text{exc}}^n$) and real space excitonic functions $F^n(\mathbf{r})$. Within the MW model, the latter represent the Fourier transforms of the envelope functions $A_{\mathbf{k}}^n$, i.e.

$$F^n(\mathbf{r}) = \frac{1}{N_{\mathbf{k}}} \sum_{\mathbf{k}} A_{\mathbf{k}}^n e^{i\mathbf{k} \cdot \mathbf{r}}. \quad (11)$$

We stress that the coefficients $A_{\mathbf{k}}^n$ used in this section are the MW approximation to those defined above for BSE. An extensive discussion on the MW approach, the related computational advantages and how it can be derived as an approximation of the BSE can be found in Ref. [35].

Borrowing the assumptions of the MW model, in par-

ticular that the excitons are extremely localized at certain points in the Brillouin zone, the K -points for TMDs, we assume that the valence-conduction momentum matrix element is constant, and simplify Eq. (3) of the main text to:

$$\mathcal{M}_{0n}^{\text{exc}} = \langle \phi_{vK} | \hat{e} \cdot \hat{p} | \phi_{cK} \rangle F^n(\mathbf{r} = 0). \quad (12)$$

This shows that whether an exciton is bright or dark, is determined by the value of its real space wavefunction at the origin. This explains why only s -like excitons are bright. Simplifications can also be done for Eq. (4) of the main text by noting that, for parabolic conduction and valence bands, $\langle \phi_{c/v\mathbf{k}} | \hat{e} \cdot \hat{p} | \phi_{c/v\mathbf{k}} \rangle = \pm k/m_{e/h}$ giving

$$\mathcal{M}_{mn}^{\text{exc}} = \left[\frac{1}{m_h} + \frac{1}{m_e} \right] \sum_{\mathbf{k}} A_{\mathbf{k}}^{m*} A_{\mathbf{k}}^n \hat{e} \cdot \mathbf{k}. \quad (13)$$

The sum in the RHS is can be expressed as the expectation value of the dipole operator, $\sum_{\mathbf{k}} A_{\mathbf{k}}^{m*} A_{\mathbf{k}}^n \hat{e} \cdot \mathbf{k} \propto (E_{b,\text{exc}}^m - E_{b,\text{exc}}^n) \int d\mathbf{r} F^{m*}(\mathbf{r}) \hat{e} \cdot \mathbf{r} F^n(\mathbf{r})$, which yield the typical hydrogen like selection rules $\Delta l = \pm 1$, with l the angular momentum quantum number.

For the calculations on the MoS₂ polaritons we used an excitonic effective mass of 0.27 a.u. which is calculated from the G_0W_0 band structure. The Keldysh screened electron-hole interaction is calculated with a polarizability $\alpha = 13.5$ a.u.. A comparison of exciton binding energies obtained with the MW model and from the solution of the BSE is shown in Fig. 7. With the MW

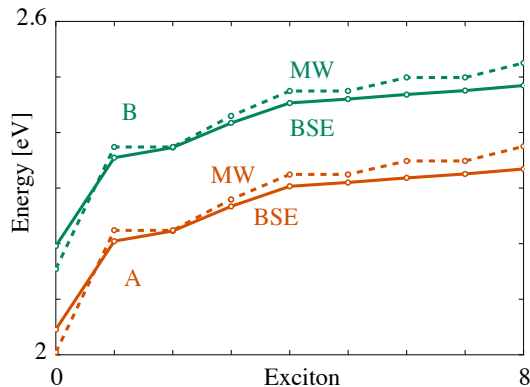


FIG. 7. Comparison of excitons energies calculated using BSE and the Mott-Wannier (MW) model.

we are then able to calculate all the excitonic quantities required in Eq. (2) of the main text and the same diagonalization procedure adopted in the QED-BSE can be performed to get the polaritonic states. Fig. 8 shows a side-by-side comparison of the polariton dispersion of MoS₂ obtained with the full QED-BSE approach and the QED-MW model. Small differences are apparent, that can be traced back to minor shifts in the exciton eigenvalues within the MW model, cf. Fig. 7. Once

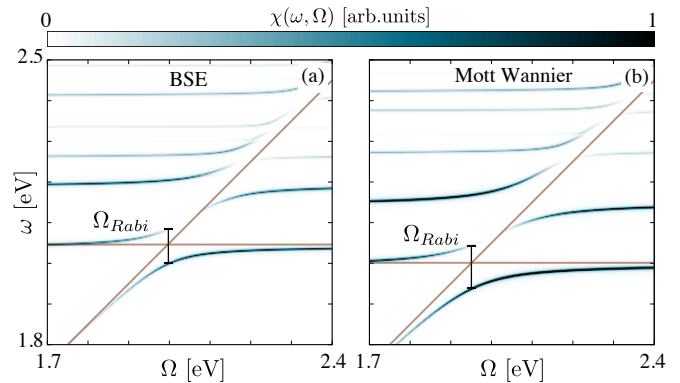


FIG. 8. Comparison of QED-BSE and QED-MW for MoS₂ and with a coupling strength of $A_0 = 0.05$ a.u.

again, the exciton-polariton dispersion is now obtained at a much lower computational cost than for the QED-BSE case and at the same time a better intuition on the photon mediated mixing of excitons can be built in terms of hydrogenic-like selection rules, according to Eqs. (9)-(13).

In the main text we used the MW model to access excitons in more complex materials, without increase in computational cost. In particular we studied the exciton-polariton dispersion in an MoS₂ monolayer encapsulated in semi-infinite dielectric with a dielectric constant κ . For this particular stacking of materials, one can readily extend the QED-MW for monolayers by including the effect of dielectric screening of the encapsulating material at three different levels: (i) the screened electron-hole Coulomb interaction is modified to [42]

$$W(\mathbf{r}, \kappa) = \frac{1}{4\alpha} [H_0(\kappa x) - N_0(\kappa x)]_{x=r/2\pi\alpha} \quad (14)$$

(ii) the bare photon dispersion in the dielectric medium changes to $\omega = \omega_c / \sqrt{\kappa}$ and (iii) the effective vector potential amplitude becomes $A_0 \rightarrow A_0 / \kappa$ [33]. The extra electronic screening due to the dielectric not only modifies the exciton binding energies but it also renormalizes the electronic gap. To estimate the electronic band gap variation as a function of κ , we take the standard assumption [3] that the change in the binding energy of the $1s$ exciton compensates the renormalization of the band gap, hence the condition $E_{\text{exc}}^{1s}(\kappa) = E_{\text{exc}}^{1s}(\kappa = 0)$ must hold. The results are shown in the main text in Fig. 4.

BIBLIOGRAPHY

- * simone.latini@mpsd.mpg.de
- † enrico.ronca@mpsd.mpg.de
- ‡ umberto.degiovannini@gmail.com
- § hannes.huebener@gmail.com
- ¶ angel.rubio@mpsd.mpg.de

- [1] S. Manzeli, D. Ovchinnikov, D. Pasquier, O. V. Yazyev, and A. Kis, *Nat. Rev. Mater.* **2**, 17033 EP (2017).
- [2] G. Wang, A. Chernikov, M. M. Glazov, T. F. Heinz, X. Marie, T. Amand, and B. Urbaszek, *Rev. Mod. Phys.* **90**, 021001 (2018).
- [3] M. M. Ugeda, A. J. Bradley, S.-F. Shi, F. H. da Jornada, Y. Zhang, D. Y. Qiu, W. Ruan, S.-K. Mo, Z. Hussain, Z.-X. Shen, F. Wang, S. G. Louie, and M. F. Crommie, *Nat. Mater.* **13**, 1091 EP (2014).
- [4] A. Ramasubramaniam, *Phys. Rev. B* **86**, 115409 (2012).
- [5] P. Cudazzo, I. V. Tokatly, and A. Rubio, *Phys. Rev. B* **84**, 085406 (2011).
- [6] J. R. Schaibley, H. Yu, G. Clark, P. Rivera, J. S. Ross, K. L. Seyler, W. Yao, and X. Xu, *Nat. Rev. Mater.* **1**, 16055 EP (2016).
- [7] J. Kim, C. Jin, B. Chen, H. Cai, T. Zhao, P. Lee, S. Kahn, K. Watanabe, T. Taniguchi, S. Tongay, M. F. Crommie, and F. Wang, *Science Adv.* **3** (2017).
- [8] G. Gao, W. Gao, E. Cannuccia, J. Taha-Tijerina, L. Balicas, A. Mathkar, T. N. Narayanan, Z. Liu, B. K. Gupta, J. Peng, Y. Yin, A. Rubio, and P. M. Ajayan, *Nano Lett.* **12**, 3518 (2012).
- [9] A. K. Geim and I. V. Grigorieva, *Nature* **499**, 419 EP (2013).
- [10] L. C. Flatten, Z. He, D. M. Coles, A. A. P. Trichet, A. W. Powell, R. A. Taylor, J. H. Warner, and J. M. Smith, *Sci. Rep.* **6**, 33134 EP (2016).
- [11] T. Chervy, S. Azzini, E. Lorchat, S. Wang, Y. Gorodetski, J. A. Hutchison, S. Berciaud, T. W. Ebbesen, and C. Genet, *ACS Photonics* **5**, 1281 (2018).
- [12] M. Slootsky, X. Liu, V. M. Menon, and S. R. Forrest, *Phys. Rev. Lett.* **112**, 076401 (2014).
- [13] X. Liu, T. Galfsky, Z. Sun, F. Xia, E.-c. Lin, Y.-H. Lee, S. Kéna-Cohen, and V. M. Menon, *Nat. Photonics* **9**, 30 EP (2014).
- [14] Z. Sun, J. Gu, A. Ghazaryan, Z. Shotan, C. R. Consideine, M. Dollar, B. Chakraborty, X. Liu, P. Ghaemi, S. Kéna-Cohen, and V. M. Menon, *Nat. Photonics* **11**, 491 EP (2017).
- [15] J. Flick, M. Ruggenthaler, H. Appel, and A. Rubio, *Proc. Nat. Ac. Sci.* (2017), 10.1073/pnas.1615509114.
- [16] J. Flick, C. Schafer, M. Ruggenthaler, H. Appel, and A. Rubio, *ACS Photonics* **5**, 992 (2018).
- [17] M. Ruggenthaler, N. Tancogne-Dejean, J. Flick, H. Appel, and A. Rubio, *Nat. Rev. Chem.* **2**, 0118 (2018).
- [18] A. Sheikhan, F. Brennecke, and C. Kollath, *Phys. Rev. A* **94**, 061603 (2016).
- [19] M. A. Sentef, M. Ruggenthaler, and A. Rubio, *ArXiv e-prints* (2018), arXiv:1802.09437 [cond-mat.supr-con].
- [20] T. Byrnes, N. Y. Kim, and Y. Yamamoto, *Nat. Phys.* **10**, 803 EP (2014).
- [21] E. E. Salpeter and H. A. Bethe, *Phys. Rev.* **84**, 1232 (1951).
- [22] M. Rohlfing and S. G. Louie, *Phys. Rev. Lett.* **81**, 2312 (1998).
- [23] M. Rohlfing and S. G. Louie, *Phys. Rev. B* **62**, 4927 (2000).
- [24] G. Onida, L. Reining, and A. Rubio, *Rev. Mod. Phys.* **74**, 601 (2002).
- [25] I. V. Tokatly, *Phys. Rev. Lett.* **110**, 233001 (2013).
- [26] M. Ruggenthaler, J. Flick, C. Pellegrini, H. Appel, I. V. Tokatly, and A. Rubio, *Phys. Rev. A* **90**, 012508 (2014).
- [27] C. Pellegrini, J. Flick, I. V. Tokatly, H. Appel, and A. Rubio, *Phys. Rev. Lett.* **115**, 093001 (2015).
- [28] J. Flick, M. Ruggenthaler, H. Appel, and A. Rubio, *Proc. Nat. Ac. Sci.* **112**, 15285 (2015).
- [29] V. Rokaž, D. M. Welakuh, M. Ruggenthaler, and A. Rubio, *J. Phys. B: At. Mol. Opt. Phys.* **51**, 034005 (2018).
- [30] J. Flick, D. M. Welakuh, M. Ruggenthaler, H. Appel, and A. Rubio, *ArXiv e-prints* (2018), arXiv:1803.02519.
- [31] T. Cao, M. Wu, and S. G. Louie, *Phys. Rev. Lett.* **120**, 087402 (2018).
- [32] Z. Ye, T. Cao, K. O'Brien, H. Zhu, X. Yin, Y. Wang, S. G. Louie, and X. Zhang, *Nature* **513**, 214 (2014).
- [33] G. Grosso and G. Parravicini, *Solid State Physics* (Elsevier Science, 2000).
- [34] L. V. Keldysh, *JETP Lett.* **29**, 658 (1979).
- [35] S. Latini, T. Olsen, and K. S. Thygesen, *Phys. Rev. B* **92**, 245123 (2015).
- [36] J. J. Mortensen, L. B. Hansen, and K. W. Jacobsen, *Phys. Rev. B* **71**, 035109 (2005).
- [37] J. Enkovaara, C. Rostgaard, J. J. Mortensen, J. Chen, M. Duak, L. Ferrighi, J. Gavnholt, C. Glinsvad, V. Haikola, H. A. Hansen, H. H. Kristoffersen, M. Kuisma, A. H. Larsen, L. Lehtovaara, M. Ljungberg, O. Lopez-Acevedo, P. G. Moses, J. Ojanen, T. Olsen, V. Petzold, N. A. Romero, J. Stausholm-Miller, M. Strange, G. A. Tritsarlis, M. Vanin, M. Walter, B. Hammer, H. Hkkinen, G. K. H. Madsen, R. M. Nieminen, J. K. Nrskov, M. Puska, T. T. Rantala, J. Schitz, K. S. Thygesen, and K. W. Jacobsen, *J. Phys.: Cond. Mat.* **22**, 253202 (2010).
- [38] J. Flick, N. Rivera, and P. Narang, *Nanophotonics* **7**, 1479 (2018).
- [39] D. Y. Qiu, H. Felipe, and S. G. Louie, *Phys. Rev. Lett.* **111**, 216805 (2013).
- [40] K. Andersen, S. Latini, and K. S. Thygesen, *Nano Lett.* **15**, 4616 (2015).
- [41] S. Haastrup, M. Strange, M. Pandey, T. Deilmann, P. S. Schmidt, N. F. Hinsche, M. N. Gjerding, D. Torelli, P. M. Larsen, A. C. Riis-Jensen, J. Gath, K. W. Jacobsen, J. J. Mortensen, T. Olsen, and K. S. Thygesen, *2D Mater.* **5**, 042002 (2018).
- [42] M. Massicotte, F. Vialla, P. Schmidt, M. B. Lundeborg, S. Latini, S. Haastrup, M. Danovich, D. Davydovskaya, K. Watanabe, T. Taniguchi, *et al.*, *Nat. Commun.* **9**, 1633 (2018).